NMR Solution Structure of Human Parathyroid Hormone(1–34)†

Julian A. Barden,*,‡ and Bruce E. Kemp§

Department of Anatomy and Histology, The University of Sydney, Sydney, N.S.W. 2006, Australia, and St. Vincent's Institute of Medical Research, Melbourne 3065, Australia

Received January 29, 1993; Revised Manuscript Received April 19, 1993

ABSTRACT: The aqueous solution structure of the biologically-active N-terminal domain of human parathyroid hormone (residues 1–34) was studied by two-dimensional proton nuclear magnetic resonance (2D NMR) spectroscopy, distance geometry, and dynamic simulated annealing. Unambiguous NMR assignments of all backbone and side chain hydrogens were made with the aid of totally correlated spectroscopy experiments, which provided through-bond ^1H–^1H connectivities, and nuclear Overhauser effect spectroscopy, which provided through-space and sequential backbone connectivities. The NMR data acquired were utilized in a distance geometry algorithm to generate a family of structures which were then refined using dynamic simulated annealing. The major structural feature evident is α-helix extending from residues Glu4 to Lys13 and from Val21 to Gln29 with a turn incorporating Asn16–Glu19 resulting in a quite globular C-terminal domain with a hydrophobic core comprising Leu15, Leu18, Trp23, and Val31. Structure–activity studies are interpreted in terms of the deduced conformation of the PTH structure with particular reference to the likely PTH receptor binding site formed primarily by the bulk of the C-terminal helix.

Homeostatic control of serum calcium is regulated by parathyroid hormone (PTH). This activity is achieved both by stimulating calcium resorption in the kidney and by resorbing calcium in the bone matrix to prevent hypocalcemia (Potts et al., 1982; Habener et al., 1984). PTH is a peptide hormone with a chain length of 84 amino acid residues with the N-terminal 34 residues retaining all the above biological activity (Potts et al., 1971; Tregear et al., 1973). Adenylate cyclase activity can be abolished in N-terminal-deleted peptides such as PTH(3–34) while receptor binding remains largely unimpaired, indicating that the activation site and the receptor binding site are located in separate domains within the segment 1–34 (Rosenblatt et al., 1977; Segre et al., 1979). Two loci in PTH(1–34) have been identified with receptor binding capacity. These reportedly involve the segment 25–34 forming a major site and the segment 10–27 forming a minor site (Rosenblatt et al., 1980; Nussbaum et al., 1980). In addition to forming a part of the receptor binding site, the segment 30–34 has been identified as possessing the capacity to exert a mitogenic effect on chondrocytes (Schlüter et al., 1989) and osteoblasts (Sömjen et al., 1990) in a cyclic AMP-independent manner.

Complete understanding of the structure–activity relationship of PTH necessitates a detailed knowledge of its tertiary structure and stability. Early attempts at investigating PTH structure in aqueous solution using one-dimensional ^1H-NMR techniques suffered from lack of resolution and an inability to assign all the resonances although the presence of some secondary structure was invoked (Bundi et al., 1976; Smith et al., 1987; Zull et al., 1987; Coddington & Barling, 1989). These conclusions were in accordance with theoretical studies of PTH structure which essentially predicted a hydrophobic cluster in the N-terminal domain (1–34) of the full-length hormone (Fiskin et al., 1977; Zull & Lev, 1980). More recently, a 2D ^1H-NMR study of PTH(1–34) was undertaken in which a complete sequence assignment was reported at pH 3 (Lee & Russell, 1989). However, no preferred secondary or tertiary structure was reported.

We have used ^1H-NMR spectroscopy to study the structure of a PTH-related protein [PTHrP(1–34)-amide][1] in aqueous solvent (Barden & Kemp, 1989) and in trifluoroethanol (Barden & Kemp, 1991; Ray et al., 1993). That work confirmed that the structure in the presence of trifluoroethanol is largely stabilized, exhibiting an N-terminal helix and a hydrophobic core in the C-terminal domain with a smaller C-terminal helix. PTHrP is a tumor product causing PTH-like symptoms of humoral hypercalcemia of malignancy (Mundy & Martin, 1982). Since its discovery (Suva et al., 1987), PTHrP has been found to share limited sequence homology with PTH in the N-terminal region and to bind to authentic PTH receptors in bone and kidney with a K_D of 0.3 nM (Kemp et al., 1987). PTHrP(1–34) contains full agonist activity, and PTHrP(7–34) and -(3–34) compete more effectively with PTHrP(1–34) for binding to PTH receptors than the equivalent PTH peptides are able to do with PTH(1–34) (McKee et al., 1988). Consequently, the backbone conformations of the two peptides are expected to be essentially identical when bound to the glycoprotein receptors, despite the possibility of the respective receptor binding sites having no sequence homology. A somewhat globular C-terminal domain was detected in PTHrP(1–34), and definite evidence of secondary structure even in aqueous solvent was determined (Barden & Kemp, 1989, 1991; Ray et al., 1993). The work presented in this paper is primarily aimed at determining the structural similarities between hPTH and hPTHrP in the receptor binding region which displays low sequence homology. Second, the study aims to establish whether PTH displays regular secondary structure in water.

† This research was supported by grants from the National Health and Medical Research Council of Australia and the Anti-Cancer Council of Victoria.

* Address correspondence to this author. Telephone: 61-02-692-2679. Fax: 61-02-552-2026.

‡ The University of Sydney.

§ St. Vincent's Institute of Medical Research.

[1] Abbreviations: DQF-COSY, double quantum filtered correlation spectroscopy; hPTH, human parathyroid hormone; hPTHrP, human parathyroid hormone related protein; NOESY, nuclear Overhauser effect spectroscopy; NMR, nuclear magnetic resonance; RMSD, root mean square deviation; TOCSY, total correlation spectroscopy.

0006-2960/93/0432-7126$04.00/0 © 1993 American Chemical Society

MATERIALS AND METHODS

Peptide Syntheses. Human PTH(1–34) was synthesized (Hodges & Merrifield, 1975) with an Applied Biosystems 430A peptide synthesizer. Amino acid derivatives protected with the *tert*-butyloxycarbonyl group in the α-amino position and benzhydrylamine resin were obtained from the Protein Research Foundation (Osaka, Japan). The Glu, Ser, and Thr side chains were protected with the benzyl group, the His side chains were protected with the dinitrophenol group, the Lys side chains were protected with the chlorobenzyl group, and the Arg side chains were protected with the nitro group. The assembled peptide underwent dinitrophenol deprotection (20% 2-mercaptoethanol in dimethylformamide) prior to cleavage from the resin with anhydrous HF containing 10% (v/v) anisole (Stewart & Young, 1966). Synthetic peptide was extracted with acetonitrile (60% v/v)/trifluoroacetic acid solvent (0.1% v/v) in water, rotary-evaporated, and lyophilized from water. Residual trifluoroacetic acid was removed using Sephadex G-10 gel filtration. The peptide was purified as described previously (Barden & Kemp, 1989).

Amino acid analyses of the HPLC-purified peptides were in close accordance with the theoretical values. Typically, a sample concentration of 3.2 mM was used with 12.8-nmol aliquots injected.

Proton NMR Spectroscopy. PTH(1–34)-amide was dissolved in a mixture of 95% H_2O/5% D_2O to give a final concentration of 3.5 mM at pH 4.1 and 300 K. Chemical shifts of the resonances and line widths were unaltered over the concentration range 0.5–5.0 mM, indicating the molecule remained monomeric at pH 4–4.5 in accordance with earlier results (Smith et al., 1987; Lee & Russell, 1989). Sample pH was adjusted with dilute HCl and NaOH and measured with an Activon BJ51130 thin-stem NMR microelectrode and a Radiometer pHM-64 meter. Values of pH reported are meter readings uncorrected for the deuterium isotope effect. Samples were placed in 5-mm precision tubes.

NMR spectra were recorded at 400 MHz in the Fourier transform mode with quadrature detection using a Bruker AMX-400 spectrometer. The 1D spectra were collected by using a 90° radio-frequency pulse of 5.7 μs. Spectral widths of 4.4 kHz were employed with a preacquisition delay of 2 s, and a total of 256 summed FIDs were collected in 16 K data points. The signal-to-noise ratios were about 350:1.

Two-dimensional (2D) phase-sensitive NMR spectra were recorded using the time proportional phase increments (TPPI) method (Redfield & Kunz, 1975). The sample was not spun in any of the experiments. A total of 512 FIDs, each consisting of 64–128 scans, were acquired with an $F2$ time domain size of 4 K. Prior to Fourier transformation, the data were zero-filled and apodized using either a shifted sine-bell (SSB) function (4–5 in $F2$ and 2.5–3.5 in $F1$) or a Gaussian multiplication in $F2$ (line broadening of –16 to –20, and GB of 0.18–0.2) and an SSB of 2–2.5 in $F1$. The 2D spectra had a final processed time domain size of 4 × 1 K through zero-filling using a Bruker X32 data station running under UNIX. COSY spectra were acquired with up to 1024 FIDs for additional resolution where necessary. Resolution in $F2$ was 1.07 Hz/point. Base lines were corrected using up to a fifth-order polynomial function. Chemical shifts were referenced to internal (trimethylsilyl)propanesulfonic acid (TSS).

Spin systems were assigned using total correlation (TOCSY) spectra obtained with an MLEV-17 pulse sequence (Bax & Davis, 1985; Griesinger et al., 1988). The mixing times were 80–100 ms, and the trim pulses were 2.5 ms. Spin-lock field strength was about 9 kHz. The water resonance was suppressed by continuous low-power (65 dB) irradiation throughout the relaxation (1.8 s) and mixing periods by utilizing O1/O2 phase coherence (Zuiderweg et al., 1986). 2D NOESY experiments (Jeener et al., 1979; Macura et al., 1981; Wüthrich, 1988) were recorded both for the purpose of obtaining proton–proton distance constraints and as an aid in making the resonance assignments sequence-specific. Spin diffusion effects were inspected by following the build-up of NOESY cross-peaks when mixing times were increased from 150 to 400 ms. A mixing time of 275 ms was used to derive proton–proton distance constraints, a suitable compromise between spin diffusion effects and cross-peak intensity.

Distance Geometry Calculations. NOE cross-peaks were separated into four distance categories depending on the intensity of the contours. Strong NOEs were given an upper distance constraint of 0.3 nm, medium NOEs were given a value of 3.5 Å, medium–weak NOEs were given a value of 4.0 Å, and weak NOEs were given a value of 4.5 Å. Corrections for pseudoatoms were applied wherever necessary. The torsion angles (ϕ) were constrained within the range –90° to –30° for all values of the coupling constant $^3J_{\alpha CHNH}$ of 5.2 Hz or lower measured from a high-resolution DQ-COSY spectrum. A total of 1000 distance geometry structures were calculated from random starting structures using the program DIANA II (Güntert et al., 1991) on a Sun 2GX Sparkstation while molecular graphics were processed using the program MidasPlus (Ferrin et al., 1988) operating on a Silicon Graphics IRIS 4D workstation.

Dynamic Simulated Annealing. The 15 structures with the lowest penalty values obtained from the DIANA calculations were refined in X-PLOR 3.0 using a dynamic simulated annealing method modified by Nilges et al. (1988). The distance geometry structures had poor potential energies since nonbonded interactions were not considered. The first stage of the simulation involved 200 cycles of energy minimization. The standard X-PLOR parameters were used for constraining the covalent geometry (Brünger, 1992). Nonbonded interactions were modeled by a repel function (=1.0) which ignored electrostatic interactions. Both the χ_1 angles and the interatomic distances were constrained by the experimental energy terms k_{cdihed} = 50 kcal·mol^{-1}·rad^{-2} and k_{NOE} = 50 kcal·mol^{-1}·Å^{-2}, with asymptote = 0.1. The second stage involved assigning very high kinetic energies for the atoms from a Maxwellian distribution corresponding to a temperature of 1000 K. The dynamic trajectory of the molecule was then followed over 50 ps in 3-fs steps followed by the tilting of the NOE restraint term or asymptote linearly to 1.0 over a further 25 ps in 3-fs steps with the increased weight on the geometry. System cooling in stage 4 was undertaken over 10 ps from 1000 K to 300 K with repel = 0.9 and C_{rep} = 4 kcal·mol^{-1}·Å^{-4}. The system was equilibrated at 300 K for 1 ps using Lennard–Jones and Coulomb potentials for nonbonded interactions (repel = 0) followed by 2000 cycles of restrained energy minimization.

RESULTS

The PTH-like activities of the synthetic peptides human PTH(1–34)-amide and human PTHrP(1–34)-amide used in the structure analyses were assayed for stimulation of [^{3}H]cAMP formation in intact UMR 106-01 cells prelabeled with [^{3}H]adenine (Moseley et al., 1987; Kemp et al., 1987). Human PTHrP exhibited higher PTH-like activity than PTH itself as expected (Figure 1). All points are means ±SEM of triplicate measurements, and the basal activity level is shown at the bottom of the figure.

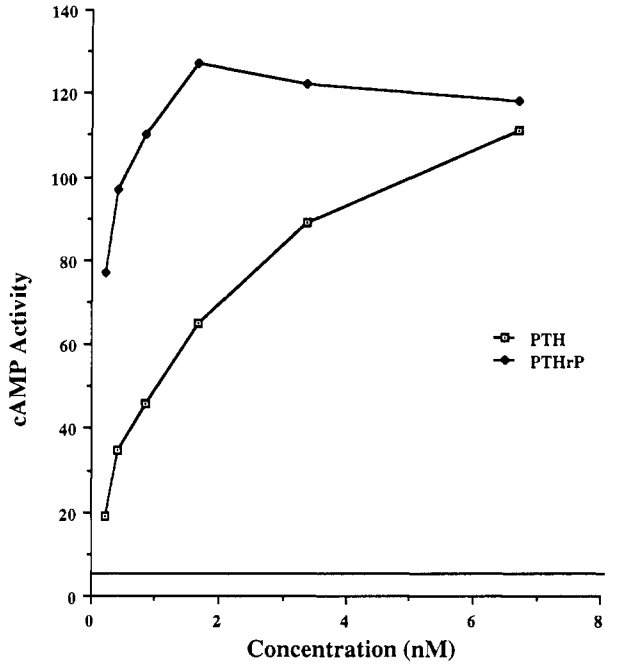

FIGURE 1: cAMP activity of the peptides human PTH(1–34)-amide and PTHrP(1–34)-amide as a function of peptide concentration in osteogenic sarcoma cells, UMR-106. The points are means ± SEM of triplicates. Activity is in cpm ($\times 10^{-3}$) of [^{3}H]cAMP. Basal activity (horizontal line) was 7000 cpm.

The "fingerprint" region of a TOCSY NMR spectrum of human PTH(1–34)-amide (Ser-Val-Ser-Glu-Ile-Gln-Leu-Met-His-Asn-Leu-Gly-Lys-His-Leu-Asn-Ser-Met-Glu-Arg-Val-Glu-Trp-Leu-Arg-Lys-Lys-Leu-Gln-Asp-Val-His-Asn-Phe-amide) recorded with a mixing time of 100 ms in H_2O is shown in Figure 2. Coherence transfers were detected even between the NH backbone and the ϵCH_2 protons on the Lys side chains separated as they are by seven bonds.

Ser1, Ile5, and Gly12 were assigned sequence specifically from the spectrum due to their uniqueness. Asp30 was assigned after a comparison was made with a spectrum acquired at pH 4.5. Trp23 and Phe34 were assigned after viewing a NOESY spectrum acquired under the same solvent conditions in which connectivities from aromatic protons to the βCH_2 protons became obvious. Thus, six spin systems were available for entry points in the sequence-specific assignment analysis using TOCSY/NOESY (Wüthrich, 1986, 1988). Sequential correlations in the N-terminal nine residues are traced out for illustrative purposes in Figure 3. In similar fashion, the sequential NH_i/NH_{i+1} cross-peaks have been boxed and labeled in Figure 4. The complete list of chemical shift values is shown in Table I.

A summary of the major observed sequential and nonsequential NOEs is shown in Figure 5 with the amino acid sequence presented in single-letter code. The thickness of the NOE line reflects the distance category, with NOE distances in the <3.0-Å range represented by the thickest lines and the <4.5-Å distances represented by the thinnest lines. The presence of an asterisk indicates the likely presence of an NOE which cannot be detected due to resonance overlap. Several NOEs of the type $H\alpha_i/NH_{i+3}$ in particular were not detectable due to overlap with other resonances. The NOEs of the type NH_i/NH_{i+1} were in general stronger than any others and combined with their universality and the relative weakness of the NOEs of the type $H\alpha_i/NH_{i+1}$ indicated a preference for helical conformation, particularly in the N-terminal region. The longer-range NOEs detected in the C-terminal region (L15δ/R20α, L15α/W23C4H, N16β/

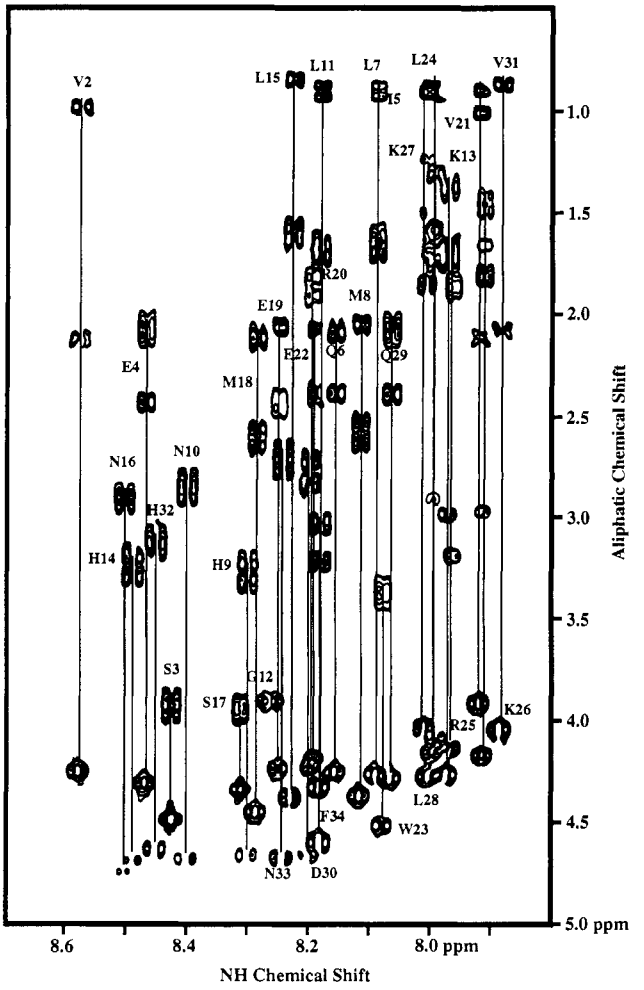

FIGURE 2: Fingerprint region of a TOCSY spectrum (mixing time 100 ms) showing all the relay scalar connectivities between the backbone NH protons and the respective side chain protons in hPTH(1–34)-amide in H_2O at a concentration of 3.5 mM, pH 4.1 and 300 K.

N33β, S17α/Q29β, M18β/V21N, R20γ/W23C4H) indicate the presence of a much more compact structure than is present in the N-terminal region, although the pattern of short- and medium-range NOEs indicates the presence of a stretch of helix.

A total of 113 useful interresidue distance constraints were used in generating the DIANA distance geometry structures. The ^3J coupling constants were measured (Figure 6). Values of 5.2 Hz or less indicated that the torsion angles (ϕ) could be loosely constrained within the range −90° to −30°. Thus, 10 torsion angle constraints were added to the 113 distance constraints in the distance geometry algorithm DIANA II (Güntert et al., 1991). The structures were generated from random starting conformations. These calculations yielded 25 structures which satisfied all the NMR distance and angle constraints. All members of the final group of nonviolated structures displayed a good covalent geometry and were free of any angle violations as well as any distance violations greater than 0.05 Å. The best 15 of these structures, those with the lowest penalty functions, were refined further using dynamic simulated annealing. No member of this family of structures had a single distance violation larger than 0.05 Å or any dihedral angle violations, and all displayed good covalent geometry. The mean RMSDs from ideal bond lengths are 0.0010 ± 0.00001 Å while the mean RMSDs from ideal bond angles are 0.1652° ± 0.0012°. The mean Lennard-Jones

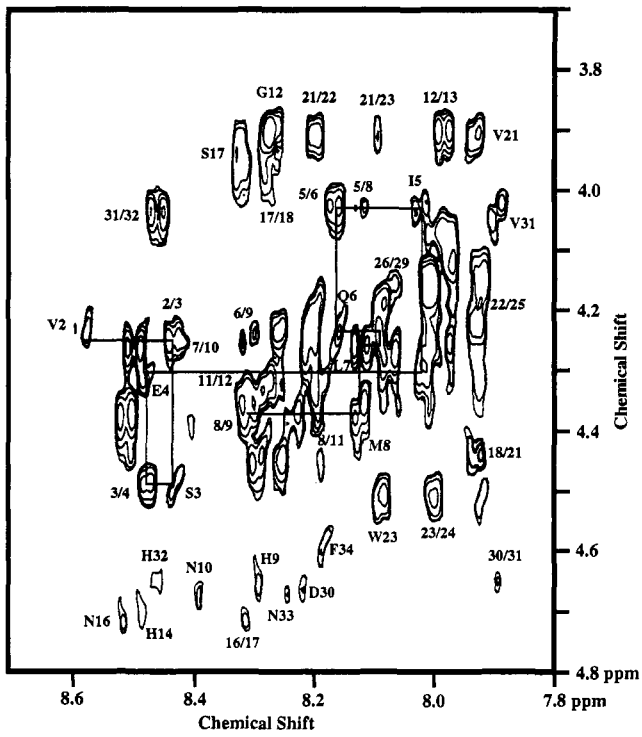

FIGURE 3: Section of a 2D NOESY spectrum of hPTH(1–34)-amide (τ_m = 275 ms) showing sequential αCH–NH connectivities. Connectivities between the N-terminal nine residues are illustrated. Solution conditions are the same as in the legend to Figure 2. Shifted sine-bell resolution enhancement was used in *F*1 and *F*2.

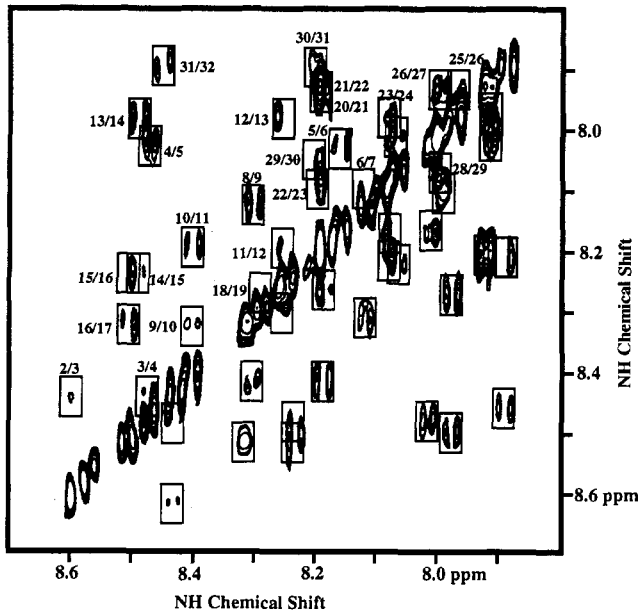

FIGURE 4: Portion of the same 2D NOESY spectrum in Figure 3 showing sequential backbone NH–NH connectivities. These cross-peaks have been boxed for clarity. Gaussian multiplication resolution enhancement was used in *F*2 to improve cross-peak differentiation.

potential of -949 ± 11 kcal·mol^{-1} indicated that the nonbonded contacts were very good.

The most prominent features in the structure of human PTH(1–34)-amide in H_2O include an α-helix in the segment Glu4–Lys13, a bend from Asn16 to Glu19, and the appearance of a second curved helix in the segment Val21–Gln29 found using a two-step superposition of the model structures. The N-terminal helix is well conserved as shown in the stereo view of an overlay of 15 of the lowest energy structures (Figure 7A). The mean RMSD between these structures in the helical region is 0.68 ± 0.30 Å. Flexibility around His14/Leu15 precluded comparisons over longer segment lengths. No NOE constraints were present within this linker region or between residues in the N-terminal domain and those in the C-terminal domain. Interactions occurring between residues either forming or adjacent to the bend and the two residues near the C-terminus, Val31 and His32, act to stabilize the C-terminal domain. These interactions reflect the presence of a hydrophobic core comprising the side chains of Leu15, Leu18, Trp23, and Val31. Surrounding the core are several charged residues including Glu19, Arg20, Glu22, Arg25, Lys26, Lys27, Asp30, and His32. A stereo view of the backbone of 12 structures superimposed over the C-terminal domain is shown in Figure 7B. The conformational space occupied by the C-terminal portion of the molecule is well-defined. The mean RMSD between these structures in the C-terminal domain is 0.26 ± 0.10 Å. The bond between Lys13 and His14 appears to be quite flexible as is the case in PTHrP (Ray et al., 1993). This may reflect an essential functional role such as enabling the easier placement of the N-terminal NH_3^+ in the signal transduction site within the receptors.

Table I: ^{1}H Assignments and Chemical Shift Data for Human PTH(1–34)-amide in H_2O, pH 4.1 at 300 K

residue	NH	αH	βH	others
Ser1		4.21	3.99, 3.99	
Val2	8.58	4.23	2.09	γCH$_3$ 0.96, 0.96
Ser3	8.43	4.47	3.94, 3.87	
Glu4	8.47	4.29	2.08, 2.02	γCH$_2$ 2.41, 2.41
Ile5	8.02	4.01	1.82	γCH$_2$ 1.47, 1.21; γCH$_3$ 0.88; δCH$_3$ 0.88
Gln6	8.16	4.23	2.06, 2.04	γCH$_2$ 2.36, 2.36; δNH$_2$ 6.86, 7.46
Leu7	8.10	4.25	1.67, 1.65	γH 1.58; δCH$_3$ 0.89, 0.85
Met8	8.12	4.35	2.02, 2.02	γCH$_2$ 2.61, 2.51; εCH$_3$ 2.03
His9	8.31	4.64	3.30, 3.20	2H 8.60; 4H 7.30
Asn10	8.41	4.66	2.85, 2.81	γNH$_2$ 7.54, 6.84
Leu11	8.19	4.30	1.68, 1.68	γCH 1.61; δCH$_3$ 0.90, 0.85
Gly12	8.27	3.88		
Lys13	7.98	4.24	1.71, 1.71	γCH$_2$ 1.37, 1.33; δCH$_2$ 1.64, 1.64; εCH$_2$ 2.96, 2.96; εNH$_3$ 7.55
His14	8.49	4.68	3.26, 3.16	2H 8.58; 4H 7.27
Leu15	8.49	4.36	1.60, 1.55	γCH 1.53; δCH$_3$ 0.83, 0.81
Asn16	8.23	4.70	2.88, 2.84	γNH$_2$ 7.58, 6.92
Ser17	8.52	4.32	3.93, 3.89	
Met18	8.29	4.43	2.10, 2.08	γCH$_2$ 2.62, 2.54; εCH$_3$ 2.05
Glu19	8.26	4.21	2.05, 2.03	γCH$_2$ 2.44, 2.38
Arg20	8.20	4.20	1.88, 1.79	γCH$_2$ 1.65, 1.58; δCH$_2$ 3.16, 3.16; NH 7.19
Val21	7.93	3.89	2.08	γCH$_3$ 0.98, 0.87
Glu22	8.20	4.17	2.05, 2.05	γCH$_2$ 2.36, 2.36
Trp23	8.08	4.49	3.38, 3.32	2H 7.23; 4H 7.57; 5H 7.11; 6H 7.19; 7H 7.49; NH 10.14
Leu24	8.00	4.05	1.66, 1.66	γH 1.56; δCH$_3$ 0.90, 0.85
Arg25	7.97	4.11	1.84, 1.84	γCH$_2$ 1.69, 1.60; δCH$_2$ 3.16, 3.16; NH 7.22
Lys26	7.92	4.14	1.79, 1.78	γCH$_2$ 1.46, 1.38; δCH$_2$ 1.63, 1.63; εCH$_2$ 2.95, 2.95; εNH$_3$ 7.53
Lys27	8.00	4.12	1.73, 1.73	γCH$_2$ 1.29, 1.27; δCH$_2$ 1.55, 1.55; εCH$_2$ 2.88, 2.88; εNH$_3$ 7.58
Leu28	8.01	4.25	1.65, 1.63	γCH 1.58; δCH$_3$ 0.88, 0.85
Gln29	8.07	4.10	2.08, 2.02	γCH$_2$ 2.36, 2.36; δNH$_2$ 6.86, 7.46
Asp30	8.21	4.64	2.80, 2.69	
Val31	7.89	4.02	2.05	γCH$_3$ 0.84, 0.84
His32	8.46	4.61	3.14, 3.08	2H 8.57; 4H 7.16
Asn33	8.25	4.65	2.73, 2.64	γNH$_2$ 7.48, 6.86
Phe34	8.19	4.57	3.18, 3.00	C3,5 7.22; C2,6 7.10

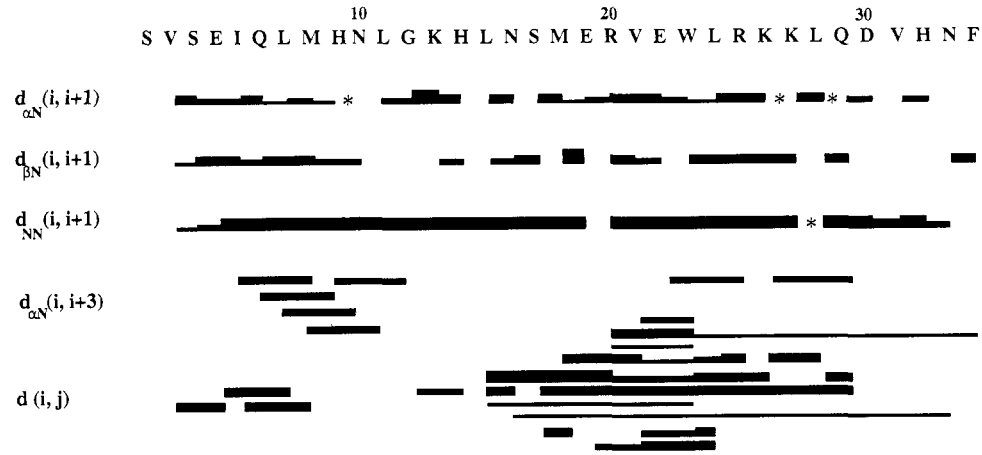

FIGURE 5: Summary of interresidue NOE connectivities observed for hPTH(1–34)-amide. The solid bars show the presence of an NOE with the thickness being proportional to the intensity of the NOE. The presence of an α-helix in the regions Glu4–Lys13 and Val21–Gln29 is strongly suggested by the pattern of NOEs. Overlapped NH resonances are shown by an asterisk. The irregular NOEs labeled as *d(i,j)*, indicating a more gobular C-terminal domain, include L15δ/R20α, L15α/W23C4H, N16β/N33β, S17α/Q29β, M18β/V21N, and R20γ/W23C4H.

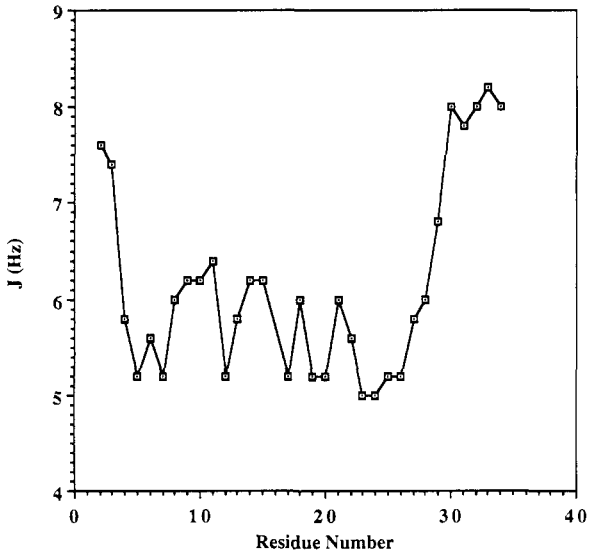

FIGURE 6: Sequence-specific vicinal J(Hα–HN) couplings estimated from a well-digitized DQ-COSY spectrum.

DISCUSSION

Theoretical analyses of the secondary structure content of PTH(1–34) carried out by by Fiskin et al. (1977), Zull and Lev (1980), and Chorev et al. (1990) predicted helices in segments 1–9 and 15–28. While there is no supporting evidence from the NMR data that residues 1–3 or 15–16 are incorporated within a helix, the remainder of the two segments 1–9 and 15–28 does occupy helical conformations. The results presented in this paper show clearly that the segment 10–13/14 remains helical in H_2O, leaving a short apparently flexible link consisting of His14/Leu15. This flexible link is a consistent feature in both PTH and PTHrP in all solution conditions tested (Ray et al., 1993). Moreover, the N-terminal helix is a consistent feature in both molecules although it appears more stable in PTH. All PTHrP analogues examined to date have revealed less stable helices.

A comparison of the C-terminal domains in the two hormones reveals a similar stretch of helix close to the C-terminus which is more stable in TFE (Ray et al., 1993). Both hormones display a turn from residues 16–19, but the orientation of the turn relative to the rest of the molecule is different, indicating that there may be a hinge between residues 21 and 22 allowing different orientations of the segment 22–34 in different environments.

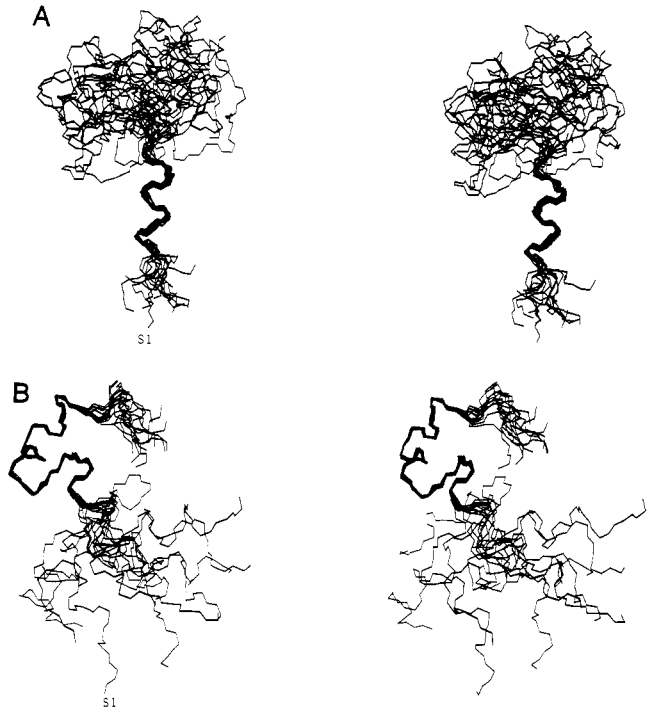

FIGURE 7: Stereo views of the backbone atoms of hPTH(1–34)-amide superimposed over the N-terminal domain 4–13 (A) and over the C-terminal domain 15–31 (B). A total of 15 structures have been superimposed over their backbone atoms with the mean RMSD equal to 0.68 ± 0.30 and 0.26 ± 0.10 Å, respectively. Three turns of helix are apparent in the N-terminus as is the flexible link around His14/Leu15 which results in an apparently unordered C-terminal domain. Nearly three turns of bent helix are apparent in the segment Val21 to Gln29 as is a bend in the segment 16–19. Leu15, Leu18, Trp23, and Val31 form a hydrophobic core surrounded by the side chains of the charged residues Glu19, Arg20, Glu22, Arg25, Lys26, Lys27, Asp30, and His32.

Previous analysis of the NMR spectrum of human PTH(1–34) at pH 3 did not reveal a preferred secondary or tertiary structure (Lee & Russell, 1989), although the side chains of Val21 and W23 interacted as found in the current work. However, our tentative investigations using fully active synthesized samples revealed significant structure at pH 4.1 in water at 300 K. The results presented in this paper are largely in agreement with several theoretical studies of PTH structure (Fiskin et al., 1977; Zull & Lev, 1980; Chorev et al., 1990). It is difficult to understand how evidence of regular secondary structure was not detected in the earlier NMR

FIGURE 8: Stereo view of the C-terminal domain 15–34 showing the side chains of Trp23, Leu24, and Leu28. Together with Val31, Leu24 and Leu28 form a hydrophobic face in this somewhat amphipathic helix. The side chain of the conserved Arg20 is immediately adjacent to the side chain of Trp23 at lower left and may form a part of a secondary binding site adjacent to the primary receptor binding site formed by the contiguous segment 24–31.

study by Lee and Russell (1989). Apart from the difference in pH, the concentration of PTH(1–34) used in the earlier study was much higher than we could obtain while still maintaining a nonaggregated solution, probably indicating that the two samples were not comparable.

A report by Klaus et al. (1991) of the structure of PTH(1–34) in 10.7% TFE reveals an extended C-terminal helix from Ser17 to Leu28, indicating that the bend (residues 16–19) is incorporated into the C-terminal helix. Strangely, these authors found the N-terminal helix ended at His9 and that Gly12 had an unusually high coupling constant which contributed to a much longer flexible linker between the N- and C-terminal helices. This structure is very different in several respects from the structure of PTHrP(1–34) determined under similar conditions (Barden & Kemp, 1991; Ray et al., 1993).

Detailed information describing the tertiary structure of PTH(1–34) provides some insight into the reasons behind the reduction in biological activity of the peptide accompanying N- and C-terminal truncations. Removal of residues Gln29 to Phe34 resulted in a 200-fold reduction in binding affinity but only 20-fold reduction in bioactivity (Segre et al., 1979) whereas PTH(1–27) was shown to be weakly active but only able to bind with an affinity 5 orders of magnitude lower than PTH(1–34) (Nussbaum et al., 1980). The receptor binding site appears to be located primarily in the C-terminal region (25–34) although some residues in the segment (14–24) may have a secondary role in receptor binding (Nussbaum et al., 1980; Caulfield et al., 1990). A stereo view of the region 15–34 is shown in Figure 8 with the side chains of Trp23, Leu24, and Leu28 added. Together with the conserved hydrophobic residue at position 31, a generally hydrophobic face is presented to the solvent by Leu24 and Leu28 with conserved charged residues at positions 25, 26, and 30 oriented along the opposite face of the somewhat amphipathic helix. The conserved Arg20 side chain is immediately adjacent to the side chain of Trp23.

PTH(3–34) binds as tightly to the receptors as does PTH(1–34) while displaying no more than 1% of full agonist activity (Segre et al., 1979). A similar finding was made with PTH(7–34) (Chorev et al., 1990). Thus, the N-terminal residues are vital only for activity but not for receptor binding. The N-terminal helix, while apparently not participating directly in binding, appears to be essential for placing the N-terminal Ser in the correct locus within the receptor separate from the primary receptor binding site. Various modifications of residue 3 in PTH (Cohen et al., 1991) demonstrated that activity fell in response to increased side chain bulk, indicating that the correct placement of the N-terminus in the receptor can be sterically impaired. The apparent hinge between the N- and C-terminal domains similarly may be required to correctly position the N-terminal helix in the various PTH receptors in order to initiate the signal transduction event. Deletion of Lys13, adjacent to the putative hinge, has been found to cause a significant reduction in binding affinity (Zull et al., 1987).

While direct sequence comparison of PTH and PTHrP indicates that the bulk of the C-terminal sequence is nonhomologous, the backbone structures of the receptor binding domains in each hormone must be well conserved. The character of the bulk of the residues in the binding region is conserved as far as being either neutral, hydrophobic, or charged. In both hormones, as revealed in this paper and in Ray et al. (1993), the structure of the putative binding domain consists of amphipathic helix to which the side chain of Arg20 appears to be immediately adjacent. Such is not the case in the extended helix found in the presence of TFE (Klaus et al., 1991).

The structural information revealed in these studies serves as the basis for ongoing investigations of the structure of the full-length proteins and provides a basis for generating mutants with altered structures and functions particularly for the purpose of producing small effective peptide and nonpeptide PTH antagonists.

ACKNOWLEDGMENT

We are grateful to Dr. Jane M. Moseley for activity measurements.

REFERENCES

Barden, J. A., & Kemp, B. E. (1989) *Eur. J. Biochem. 184*, 379–394.
Barden, J. A., & Kemp, B. E. (1991) *Life Sci. 3*, 56–60.
Bax, A., & Davis, D. G. (1985) *J. Magn. Reson. 65*, 355–360.
Brünger, A. T. (1992) *X-PLOR*, Version 3.0, User Manual, Yale University, New Haven, CT.
Bundi, A., Andreatte, R., Rittel, W., & Wüthrich, K. (1976) *FEBS Lett. 64*, 126–129.
Caulfield, M. P., McKee, R. L., Goldman, M. E., Duong, L. T., Fisher, J. E., Gay, C. T., DeHaven, P. A., Levy, J. J., Roubini, E., Nutt, R. F., Chorev, M., & Rosenblatt, M. (1990) *Endocrinology 127*, 83–87.
Chorev, M., Goldman, M. E., McKee, R. L., Roubini, E., Levy, J. J., Gay, C. T., Reagen, J. E., Fisher, J. E., Caporale, L. H., Golub, E. E., Caulfield, M. P., Nutt, R. F., & Rosenblatt, M. (1990) *Biochemistry 29*, 1580–1586.
Coddington, J. M., & Barling, P. M. (1989) *Mol. Endocrinol. 3*, 749–753.
Cohen, F. E., Strewler, G. J., Shannon Bradley, M., Carlquist, M., Nilsson, M., Ericcson, M., Ciardelli, T. L., & Nissenson, R. A. (1991) *J. Biol. Chem. 266*, 1997–2004.
Ferrin, T. E., Huang, C. C., Jarvis, L. E., & Langridge, R. (1988) *J. Mol. Graphics 6*, 13–27.
Fiskin, A. M., Cohn, D. M., & Peterson, G. S. (1977) *J. Biol. Chem. 252*, 8261–8268.
Griesinger, C., Otting, G., Wüthrich, K., & Ernst, R. R. (1988) *J. Am. Chem. Soc. 110*, 7870–7872.
Güntert, P., Braun, W., & Wüthrich, K. (1991) *J. Mol. Biol. 217*, 517–530.
Habener, J. F., Rosenblatt, M., & Potts, J. T., Jr. (1984) *Physiol. Rev. 64*, 985–1053.
Hodges, R. S., & Merrifield, R. B. (1975) *Anal. Biochem. 65*, 241–272.
Jeener, J., Meier, B. H., Bachmann, P., & Ernst, R. R. (1979) *J. Chem. Phys. 71*, 4546–4553.
Kemp, B. E., Moseley, J. M., Rodda, C. P., Ebeling, P. R., Wettenhall, R. E. H., Stapleton, D., Diefenbach-Jagger, H.,

Ure, F., Michelangeli, V. P., Simmons, H. A., Raisz, L. G., & Martin, T. J. (1987) *Science 238*, 1568–1570.
Klaus, W., Dieckmann, T., Wray, V., Schomburg, D., Wingender, E., & Mayer, H. (1991) *Biochemistry 30*, 6936–6942.
Lee, S. C., & Russell, A. F. (1989) *Biopolymers 28*, 1115–1127.
Macura, S., Huang, Y., Sutter, D., & Ernst, R. R. (1981) *J. Magn. Reson. 43*, 259–281.
McKee, R. L., Goldman, M. E., Caulfield, M. P., DeHaven, P. A., Levy, J. J., Nutt, R. F., & Rosenblatt, M. (1988) *Endocrinology* 122, 3008–3010.
Moseley, J. M., Kubota, M., Diefenbach-Jagger, H. D., Wettenhall, R. E. H., Kemp, B. E., Suva, L. J., Rodda, C. P., Ebeling, P. R., Hudson, P. J., Zajac, J. D., & Martin, T. J. (1987) *Proc. Natl Acad. Sci. U.S.A. 84*, 5048–5052.
Mundy, G. R., & Martin, T. J. (1982) *Metabolism 31*, 1247–1277.
Nilges, M., Clore, G. M., & Gronenborn, A. M. (1988) *FEBS Lett.* 239, 129–136.
Nussbaum, S. R., Rosenblatt, M., & Potts, J. T., Jr. (1980) *J. Biol. Chem. 255*, 10183–10187.
Potts, J. T., Jr., Tregear, G. W., Keutmann, H. T., Niall, H. D., Sauer, R. T., Deftos, L. J., Dawson, B. F., Hogan, M. L., & Aurbach, G. D. (1971) *Proc. Natl. Acad. Sci. U.S.A. 68*, 63–67.
Potts, J. T., Jr., Kronenberg, H. M., & Rosenblatt, M. (1982) *Adv. Protein Chem. 35*, 323–396.
Ray, F. R., Barden, J. A., & Kemp, B. E. (1993) *Eur. J. Biochem.* 211, 205–211.
Redfield, A., & Kunz, S. D. (1975) *J. Magn. Reson. 19*, 250–254.
Rosenblatt, M., Callahan, E. N., Mahaffey, J. E., Pont, A., & Potts, J. T., Jr. (1977) *J. Biol. Chem. 252*, 5847–5851.
Rosenblatt, M., Segre, G. V., Tyler, G. A., Shepard, G. L., Nussbaum, S. R., & Potts, J. T., Jr. (1980) *Endocrinology 107*, 545–550.
Schlüter, K. D., Hellstern, H., Wingender, E., & Mayer, H. (1989) *J. Biol. Chem. 264*, 11087–11092.
Segre, G. V., Rosenblatt, M., Reiner, B. L., Mahaffey, J. E., & Potts, J. T., Jr. (1979) *J. Biol. Chem. 254*, 6980–6986.
Smith, L. M., Jentoft, J., & Zull, J. E. (1987) *Arch. Biochem. Biophys. 253*, 81–86.
Sömjen, D., Binderman, I., Schlüter, K. D., Wingender, E., Mayer, H., & Kaye, A. M. (1990) *Biochem. J. 272*, 781–785.
Stewart, J. M., & Young, J. P. (1966) *Solid State Peptide Synthesis*, pp 44 and 66, W. H. Freeman, San Francisco.
Suva, L., Winslow, G. A., Wettenhall, R. E. H., Hammonds, R. G., Moseley, J. M., Diefenbach-Jagger, H., Rodda, C. P., Kemp, B. E., Rodriguez, H., Chen, E., Hudson, P. J., Martin, T. J., & Wood, W. I. (1987) *Science 237*, 893–896.
Tregear, G. W., van Rietschoten, J., Greene, E., Keutmann, H. T., Niall, H. D., Reit, B., Parsons, J. A., & Potts, J. T., Jr. (1973) *Endocrinology 93*, 1349–1353.
Wüthrich, K. (1986) *NMR of Proteins and Nucleic Acids*, J. Wiley and Sons, New York.
Wüthrich, K. (1988) *Science 243*, 45–50.
Zuiderweg, E. R. P., Hallenga, K., & Olejniczak, E. T. (1986) *J. Magn. Reson. 70*, 336–343.
Zull, J. E., & Lev, N. B. (1980) *Proc. Natl. Acad. Sci. U.S.A. 77*, 3791–3795.
Zull, J. E., Smith, L. M., Chuang, J., & Jentoft, J. (1987) *Mol. Cell. Endocrinol. 51*, 267–271.